Journal of Applied Polymer Science

# A highly oriented poly(3,4-ethylenedioxythiophene) film: Facile synthesis and application for supercapacitor

**Huan Yang, Ye Liu, Zhongde Wang, Yiming Liu, Haiyan Du, Xiaogang Hao**
Department of Chemical Engineering, Taiyuan University of Technology, Taiyuan 030024, China
Correspondence to: Z. Wang (E-mail: wangzhongde@tyut.edu.cn) and
X. Hao (E-mail: xghao@tyut.edu.cn or tyutxghao@hotmail.com)

**ABSTRACT:** A single crystal poly(3,4-ethylenedioxythiophene) (PEDOT) film with highly oriented arrangement has been fabricated from an aqueous solution by a novel unipolar pulse electropolymerization method. Film formation mechanism was proposed based on the in situ mass change during electropolymerization process measured by the electrochemical quartz crystal microbalance. The compositions, morphology and crystal structure of the fabricated films are characterized by Fourier transfer infrared spectroscopy, scanning electron microscopy, and X-ray diffraction, respectively. It is found that the prepared PEDOT film on carbon nanotubes (CNTs)-modified electrode with a spongy dendritic structure possesses outstanding electroactivity, high specific capacitances (239.1 $F{\cdot}g^{-1}$, including the specific capacitances of CNTs which is 21.4 $F{\cdot}g^{-1}$), and excellent cycling stability with 7.3% decay from its initial capacitance over 10,000 cycles. © 2016 Wiley Periodicals, Inc. J. Appl. Polym. Sci. **2016**, *133*, 43418.

**KEYWORDS:** electrochemistry; functionalization of polymers; morphology; surfaces and interfaces; structure–property relations

Received 18 September 2015; accepted 3 January 2016
**DOI: 10.1002/app.43418**

## INTRODUCTION

Since Shirakawa *et al.*[1] discovered electrically conductive polyacetylene, conducting polymers (CP), which are often referred as synthetic metals, have been widely investigated for their application in different fields, such as solar cells,[2,3] antistatic and anticorrosion materials,[4] polymer electrochromic devices,[5,6] catalyst support,[7] electrochemical supercapacitor,[8–10] and electrochemical sensors.[11–15] Among the CPs that have been developed over the past 4 decades, those based on polyanilines, polypyrroles, and polythiophenes have attracted great attention.

Poly(3,4-ethylenedioxythiophene) (PEDOT),[16] first synthesized in the 1990s by Bayer AC,[17–19] is recognized as one of the most promising conducting polymers for electrochemical supercapacitor due to its remarkable conductivity (up to 500 $S\ cm^{-1}$),[20] superior chemical and mechanical stability. Supercapacitor can be used as the charge storage device and generally possesses rapid charge–discharge rate, long cycle life, and high reliability.[21,22] Although PEDOT is considered as a good material for capacitor, its specific capacitance needs to be improved more in order to satisfy the requirements of supercapacitor.[8,9] In recent years, many efforts have been devoted for this purpose. Huang *et al.* prepared PEDOT powder with globular-like shape and an average diameter of 1.5 $\mu$m by oxidative polymerization method, in which imidazole (Im) was used as inhibitor. They fabricated a capacitor using this kind of PEDOT powder and obtained a specific capacitance of 124 $F{\cdot}g^{-1}$.[23] Pandey *et al.* prepared PEDOT film composed of small grains using current pulse polymerization method and obtained a capacitor with a specific capacitance of[24] 85 $F{\cdot}g^{-1}$ and then, they enhanced the specific capacitance to[25] 154.5 $F{\cdot}g^{-1}$ by coating it on carbon paper electrode. Xiao *et al.* electropolymerized dense nanomeadows PEDOT by using the pulse potentiostatic method with pulse-on and pulse-reversal period, but no data on its specific capacitance was reported.[26] Ryu *et al.*[27] mixed PEDOT with active carbon powder and used it as electrode material and obtained a specific capacitance of 56 $F{\cdot}g^{-1}$ after 1000 cycle.

In general, the capacity of electrochemical supercapacitor could be controlled by the microstructure of the interface between electrode and electrolyte solution.[28] This is the motivating factor for fabricating porous electrode with nanostructure for supercapacitor application. For PEDOT, when it is prepared by cyclic voltammeter (CV), traditional pulse polymerization and potentiostatic (PS) method, the structures with compact globular or conjoint irregular strings morphology are generally formed, and low specific capacitances ranged from 90 to 180 $F{\cdot}g^{-1}$ and poor cycle stability are obtained when they are used as supercapacitor materials.[29–33] The energy storage capability in supercapacitor

Additional Supporting Information may be found in the online version of this article.

materials depends on the reversible electrochemical reaction in which doping/undoping of ions occurs.[34] As such, dense surface morphology of the polymer matrix will lower the specific capacitance. Therefore, it is necessary to control the micro and nanostructure of electrode in order to improve the specific capacitance and stability of the target supercapacitor.

In the present study, a try was performed to investigate the relationship between the microstructure of PEDOT and its electrochemical property when used as supercapacitor material. PEDOT film was grown on carbon nanotube (CNT)-modified platinum substrate via the unipolar pulse electropolymerization (UPEP) method developed by our group. It is expected to result in an extremely high effective surface area and improve its specific capacitance. In our previous studies, nanorod polyaniline film, highly stable polypyrrole film and NiHCF/CS/CNTs composite film with high electroactivity were successfully fabricated using this method.[8,9,35] Different from traditional current or potential pulse polymerization, in this method, a potential is fixed and current can be generated during the on-time period, followed by an off-time period, in which no current is allowed to flow. Based on the unique kinetics of EDOT nucleation and characteristics of UPEP method, PEDOT film with higher degree of dopant ions and special nanostructure could be achieved. Furthermore, since CNTs is found to be an appropriate medium bonding active material and matrix.[36] In this work, CNTs-polyvinylidene fluoride (PVDF)-modified Pt electrode was considered to fix PEDOT film on matrix, in which PVDF could cohere CNTs fibers together, which can further increase the adhesive force between CNTs and Pt sheet. The performance characteristics of the obtained highly oriented spongy dendritic structure PEDOT-based electrodes (UPEP S−PEDOT) were evaluated using CV, galvanostatic charge–discharge, cycling stability and electrochemical impedance spectra (EIS). For comparison, PEDOT film was also prepared by PS method (abbreviated as PS PEDOT) and evaluated under the same conditions.

## EXPERIMENTAL

### Materials

3,4-Ethylenedioxythiophene (EDOT>97%) purchased from Sigma–Aldrich was stored in nitrogen atmosphere under 8 °C prior to use. Reagent grade sodium dodecyl sulfate (SDS, $CH_3(CH_2)_{11}SO_3Na$) from Merck was used as surfactant. All solutions were prepared using ultra-pure water (Millipore 18.2 MΩ cm).

### Preparation of Conducting Polymer-Coated CNT-Modified Matrix

70 mg PVDF was dissolved in 5 mL dimethyl formamide (DMF) under 70 °C, then 25 mg CNTs powder[37] was dispersed in it with ultrasonic cell disrupting for 30 min to obtain uniform suspension. Pt sheet was used as working electrode (using PVC tape to limit effective surface area of 0.5 $cm^2$). 10 $\mu$L droplet of CNTs/PVDF suspension was syringe dispensed on the Pt sheet and 1 $\mu$L droplet of CNTs/PVDF suspension for electrochemical quartz crystal microbalance (EQCM) golden disc, then dried for 2 days in oven at 30 °C. A Sartorius balances of model CP22 5D-OCE with 0.01 mg sensitivity was used for weighing the working electrode after drying. An electrolyte of 0.02 M EDOT + 0.01 M SDS + 0.1 M $H_2SO_4$ aqueous solution was used for PEDOT preparation. Considering that monomers of EDOT have extremely low solubility in water, SDS was used as the surfactant to form micelles as well as doping agent. The addition of SDS at different concentrations could influence the gel-forming properties of EDOT monomers. It is found that 0.02 M EDOT possesses the optimal gel-forming properties and electrochemical activity in the presence of 0.1 M SDS, which are described in Supporting Information Figures S1 and S2. The mixture was stirred for 2 h to make the monomer well-distributed until a clear mixed solution was obtained.

### Electropolymerization of PEDOT Film

Electrochemical preparation and characterization of the PEDOT film were performed with a VMP3 Potentiostat (Princeton) operated with a computer interface using EC-Lab application software for control and data handling. The electrolyte solution of the monomer was prepared by dissolution of 0.02 M EDOT, 0.01 M SDS, and 0.1 M $H_2SO_4$ in aqueous solution. The electrochemical polymerization was then performed by a three electrode system equipped with saturated calomel electrode as reference electrode, platinum wire as counter electrode, and CNT-modified platinum sheet as working electrode. After the electrochemical deposition of the required quantity of PEDOT, the electrode was rinsed with ultrapure water, dried at 30 °C and weighed. The operation parameters for the electrochemical deposition of PEDOT employing UPEP method were 1.1 V, on-time of 1 s and off-time of 1 s, 5400 times. Then the PEDOT films were washed completely with ultrapure water and weighted after drying. In the PS method, a constant voltage (1.1 V) was applied to the working electrode, where the same solution as that in the UPEP method was used. However, the polymerization time was set at 70 min so that the total mass of PEDOT deposited was the same as that obtained by the UPEP method. The mass of PEDOT film is 0.8 mg, because the specific capacitance value is the highest when PEDOT film is 0.8 mg (Supporting Information Figures S3 and S4).

### Characterization and Measurements of PEDOT Film

Morphology of the film was examined by a scanning electron microscope (SEM, LEO438VP), X-ray diffraction (XRD, Shimadzu/XRD-6000) and the chemical structure was analyzed by Fourier transform infrared spectrometer (FT-IR, Nicolet 6700). Electrochemical properties of the film were measured by CV, galvanostatic charge/discharge and electrochemical impedance spectroscopy techniques in the 0.3 M $HClO_4$ and 0.1 M $NaClO_4$ solutions, which was reported to be a better electrolyte than other electrolytes for obtaining stable capacitance values of conducting polymers.[29,38] The optimal ratio of $HClO_4/NaClO_4$ is discussed in Supporting Information Figure S5. Electroactivity and specific capacitance were investigated by galvanostatic charge/discharge from −0.2 to 0.7 V with an applied constant current density of 0.7 mA $cm^{-2}$. EIS measurement was carried out with frequencies varying from 100 kHz to 1 mHz, using AC amplitude of 10 mV at open circuit potentials.

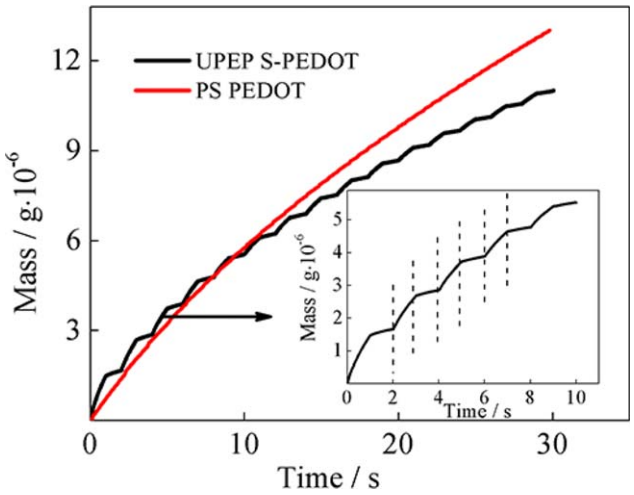


**Figure 1.** Mass responses of UPEP S–PEDOT and PS PEDOT films prepared on CNT-modified golden disc in three-electrode system. The inset is an enlargement of the mass responses of UPEP S–PEDOT film during the initial 5 pulse. PS conditions: 1.1 V, 30 s. Pulse conditions: 1.1 V pulse potential, 1 s on-time and 1 s off-time, and 15 pulse numbers. [Color figure can be viewed in the online issue, which is available at wileyonlinelibrary.com.]

## RESULTS AND DISCUSSION

### Electropolymerization Process of PEDOT Films

A suitable tool to trace the mass change in electropolymerization and electrochemical measurement process of conducting polymers is EQCM. This technique involves using quartz crystal with golden disc coated on both sides and one side used as working electrode. In present work, a 1-$\mu$L droplet of CNTs/PVDF suspension was syringe dispensed on the center spot of golden disc. Then, the piezoelectric property of quartz crystal was utilized to calculate the mass change (down to nanogram levels) of the polymer attached on the electrode surface according to the Sauerbrey equation.[39] The EQCM results presented in Figure 1 shows the first 30 s mass/time transient curves of PEDOT films on CNT-modified golden disc in three-electrode system employing UPEP and PS method respectively. As shown in the inset of Figure 1, there is a significant mass increase of UPEP S−PEDOT during the first on-time, but almost no mass change occurs in off-time, which means that EDOT monomers are polymerized dramatically during on-time. PEDOT is generally polymerized via cationic free radical polymerization. As such, at the first on-time pulse, EDOT monomers could be oxidized under 1.1 V potential, then $EDOT^{+\bullet}$ radical cations sites were generated at 2, 5 sites of monomers.[24,40,41] More and more active sites could contact each other and promote the cationic free radical polymerization to occur. With the doping of $SDS^{-}$ anion for the neutralization of the charge, the polymerization will be accomplished.[40] During off-time, there still exist lots of $EDOT^{+\bullet}$ radical cations on the PEDOT chain, which have no time to participate in the polymerization reaction. These active sites could be reduced through oxidizing dissociative EDOT monomers in the solution. Some of these active sites loss their oxidation activity so that PEDOT chains hardly grow at the following on-time pulse. The direction of next PEDOT chain growth should be ascertained by where the more $EDOT^{+\bullet}$ radical cations will be retained. After several times of pulse, a cusp could be formed, which will accelerate the growth of PEDOT chain along the direction of the tip until PEDOT chains appear as nanorod. Afterward, several separated branches will be divided from the previous nanorod. Ultimately, a dendritic structure appears. Unlike UPEP S−PEDOT, the mass of PS PEDOT film always increases over time at a constant rate. In the potentiostatic method, there are two platforms of current during the polymerization process as shown in Supporting

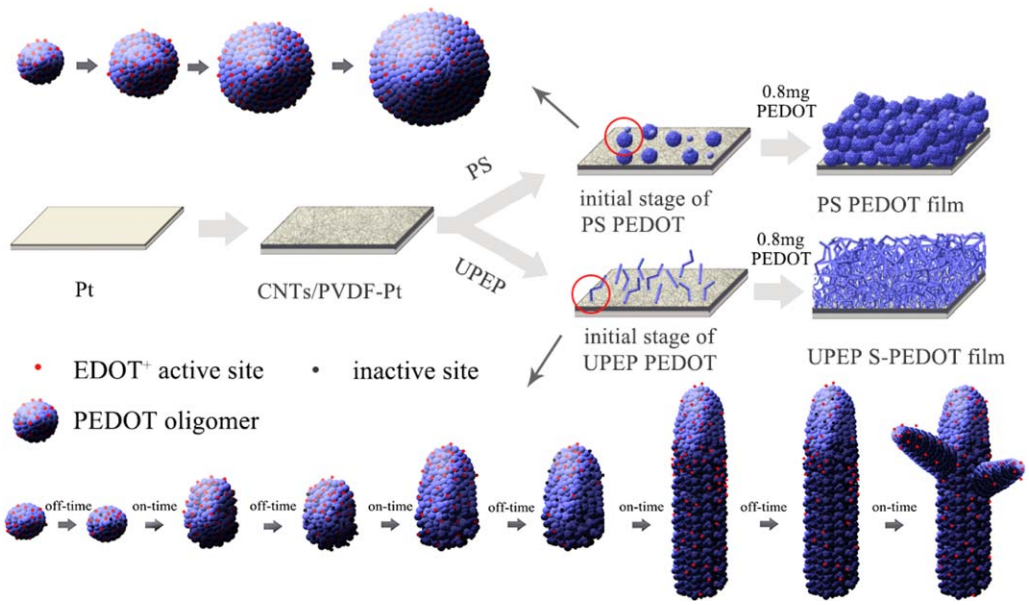


**Figure 2.** Schematic representation of the growth pattern of PS PEDOT and UPEP S–PEDOT. [Color figure can be viewed in the online issue, which is available at wileyonlinelibrary.com.]

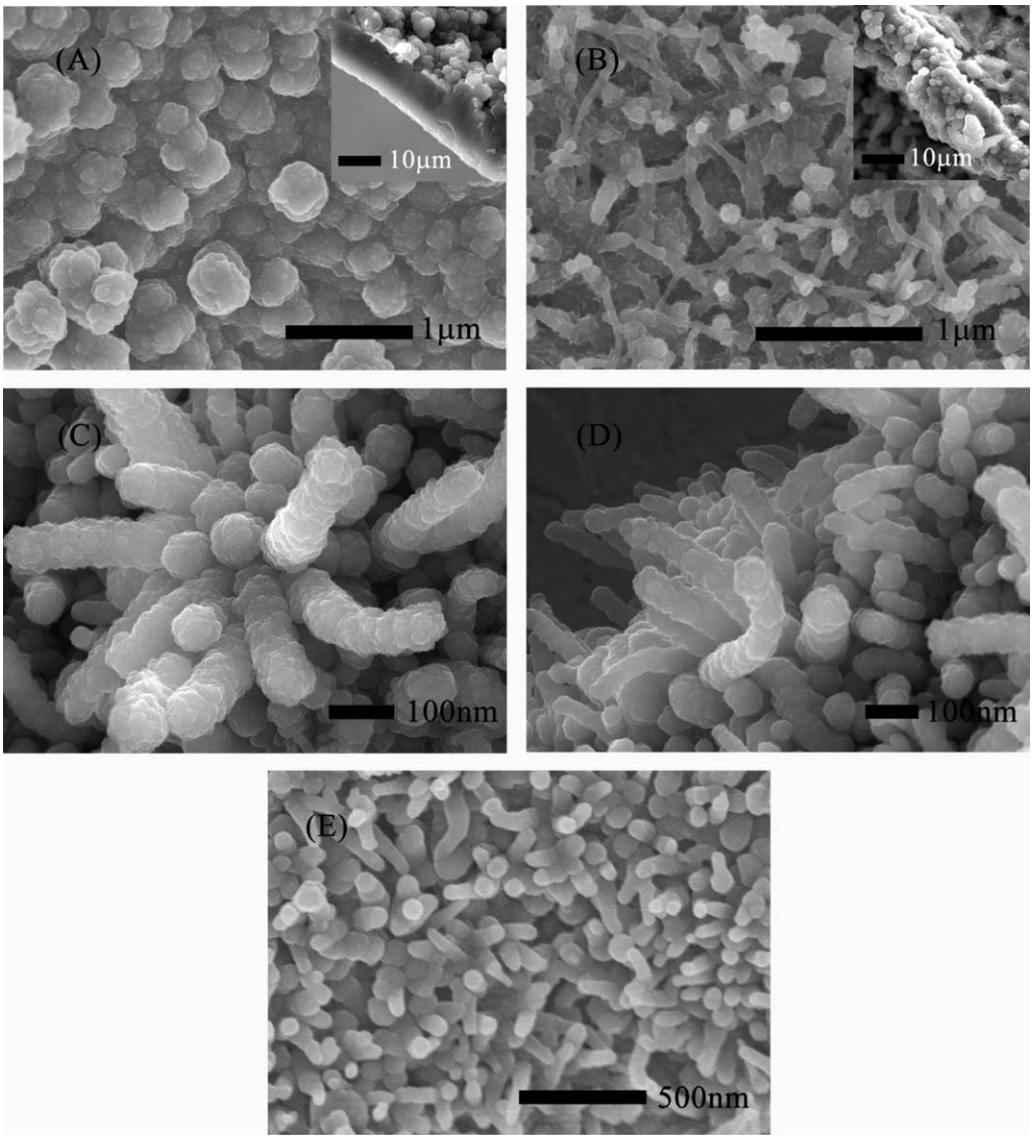


**Figure 3.** The Scanning electron micrographs of the PS PEDOT (A), UPEP S–PEDOT (B) with cross-section enlarged view inset. The condition for preparing PS PEDOT film: 1.1 V, 70 min. The condition for preparing UPEP S–PEDOT film: 1.1 V pulse potential, 1 s on-time and 1 s off-time, 5400 pulse numbers. Top view (C) and side view (D) of UPEP S–PEDOT connection joints. Scanning electron micrographs of UPEP S–PEDOT (E) in incipient stage.

Information Figure S6. The initial platform exists in the first 100 s corresponding to the formation of PEDOT nuclei. The current of second platform is lower than the initial stage corresponding to the growth of the polymer where current dose not vary with time. At the beginning of the polymerization, EDOT monomer is activated and linked together with lots of $EDOT^{+\bullet}$ radical cations on the chain, then PEDOT chains twine around each other to form nuclei.[33] In the following polymerization process, the current is tending toward stability. The monomers keep growing on the surface of the nuclei under the constant voltage. Due to three-dimensional growth pattern, the PS PEDOT nucleus grows to form a solid and round structure. The mechanism of nucleation and growth is shown in Figure 2. The PEDOT electrode with a spongy dendritic structure obtained by UPEP should be more suited for high performance supercapacitors.

**Morphology of PEDOT Films**

The morphologies of PEDOT films obtained with UPEP and PS methods were examined by SEM, as shown in Figure 3. PS PEDOT film (A) is globular-like particles aggregated together into a ball-like structure with a diameter of 0.2 $\mu$m.[33,42] The cross section of PS PEDOT is imporous and compact as shown in Figure 3(A) inset. UPEP S–PEDOT film (B) reveals a spongy dendritic structure composed of uniform distributed nanorods with diameter less than100 nm and length ranging from 300 to 500 nm. As shown in the inset of Figure 3(B), the cross section of UPEP S–PEDOT is composed of several crosswise dendritic nanorods with small interspaces between the rods. Side view and top view of UPEP S–PEDOT connection joints enlarged view are shown in Figure 3(C,D). One can see the dendritic-like structure of UPEP S–PEDOT clearly from these two angles, therefore, it is beneficial for ion diffusion in UPEP S–PEDOT

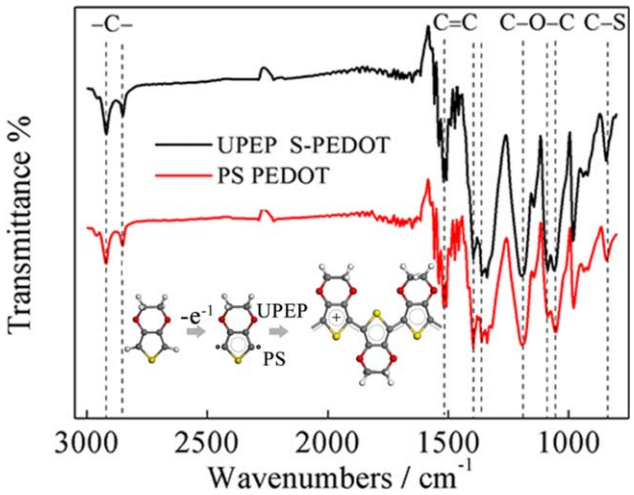


**Figure 4.** FTIR spectra of UPEP S–PEDOT and PS PEDOT films. [Color figure can be viewed in the online issue, which is available at wileyonlinelibrary.com.]

film. In the case of incipient polymerization, the morphology of PEDOT film prepared by UPEP with only 10 times pulses is presented in Figure 3(E). PEDOT film prepared under a transitory action of pulsing voltage has a coralloid structure erected on the matrix. Based on the mechanism of nucleation and growth of UPEP S−PEDOT illustrated in Figure 2, the EDOT monomers should be oxidized to radical cations and subsequently germinated into PEDOT nanorod. After multiple times of pulses, lots of pronged nanorods grow and branch to form a sponge dendritic structure.

### FT-IR Spectra of PEDOT Films

FT-IR spectra of UPEP S−PEDOT and PS PEDOT are given in Figure 4. UPEP S−PEDOT and PS PEDOT exhibit almost the same FTIR spectrum. The vibrations at 1519, 1400, and 1362 $cm^{-1}$ are corresponding to the C−C and C=C stretching in the thiophene ring. Peaks at 1197, 1088, and 1052 $cm^{-1}$ are assigned to the stretching modes of C−O−C ethylenedioxy group. And band at 840 $cm^{-1}$ could be ascribed to the vibration modes of C−S bond in the thiophene ring.[43–45] The two strong peaks around 2914 and 2846 $cm^{-1}$ were attributed to the stretching vibration mode of methylene, indicating that surfactant SDS has been doped into the chains of PEDOT.[46,47] Combining with the similar bonding structure observed from FT-IR spectroscopic analysis, the result indicates that UPEP S−PEDOT and PS PEDOT are formed by the same oligomers. The structure formula of PEDOT formation is shown in the inset of Figure 4.

### XRD Pattern of UPEP S–PEDOT and PS PEDOT Films

XRD was used to probe the crystallographic ordering of PEDOT films deposited with UPEP and PS method, and results are shown in Figure 5. The PEDOT crystal structure changes markedly with deposition method. UPEP S−PEDOT does not yield any characteristic peaks except for the strong diffused angle peak at $2\theta$ ~25.7°, which can be attributed to the interchain planar ring stacking.[42,44,48] Only the (020) reflection is present, suggesting crystalline laminae grow along the b-axis perpendicular to the substrate sheet,[43] which is shown in the schematic illustration of the crystal arrangement in Figure 5. This indicates that UPEPS−PEDOT is highly oriented. Besides the characteristic peak at nearly $2\theta$ ~25.7°, the diffraction peaks with low intensity at $2\theta$ ~10.1° occur in the case of PS PEDOT which corresponds to (200) reflection.[49,50] These diffraction peak positions and intensities conform to the randomly oriented PEDOT material stacking along the axis a and b,[43] which is shown in Figure 5. This phenomenon indicates that PS PEDOT is not highly oriented. According to the Bragg's law, the corresponding lattice parameters are calculated to be $a = 17.52$ Å and $b = 6.92$ Å. The detail of lattice parameter values is provided in Supporting Information Table S2. In the PS method, PEDOT films exhibit a random polycrystalline structure, whereas UPEP method may promote a more favorably aligned crystal structure. These results illustrate that the lower rate of polymerization enhances crystallinity.[51] On the whole, polymerization rate of UPEP method is much lower than PS method due to the existence of the off-time period. UPEP S−PEDOT combined with the intermittent polymerization kinetics possesses more regular polymer chain stacking compared to PS PEDOT.[23] In the polymerization process of UPEP S−PEDOT, the $SDS^-$ anions could be replenished within the electric double layer during off-time.

### Electrochemical Characterization

**Electroactivity with EQCM.** The electrochemical performance of the PEDOT electrodes was evaluated by CV. The CV curves for UPEP S−PEDOT as well as PS PEDOT over the voltage range from −0.2 to 0.7 V under 20 mV $s^{-1}$ scan rate in 0.3 M $HClO_4$, 0.1 M $NaClO_4$ aqueous solution are shown in Figure 6(A). The shape of the CV plots of two films closely resembles a rectangle, showing its ideal capacitor behavior.[24] Comparing to the PS PEDOT film, the current of UPEPS−PEDOT film is higher within the same potential range, indicating that the UPEPS−PEDOT film has better electroactivity at the same scan rate. The EQCM results for the CV of PEDOT in an aqueous

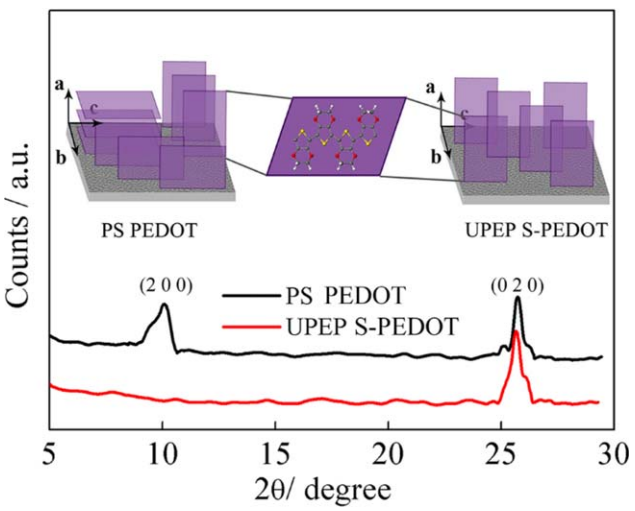


**Figure 5.** X-ray diffraction spectra and schematic illustration of the crystal arrangement of UPEP S–PEDOT, PS PEDOT films deposited on CNT-modified platinum substrate. [Color figure can be viewed in the online issue, which is available at wileyonlinelibrary.com.]

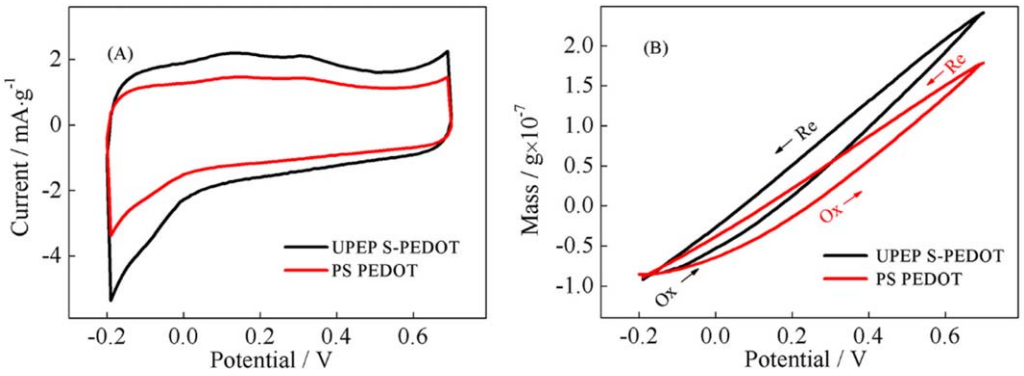


**Figure 6.** Cyclic voltammetric (A) and mass responses (B) of UPEP S–PEDOT and PS PEDOT films prepared on CNT-modified golden disc in three-electrode system. Cyclic voltammetric condition: electrolyte, 0.3 M $HClO_4$, 0.1 M $NaClO_4$; scan rate, 20 mV $s^{-1}$; scan range, −0.2 to 0.7 V. [Color figure can be viewed in the online issue, which is available at wileyonlinelibrary.com.]

solution of 0.3 M $HClO_4$, 0.1 M $NaClO_4$ after several cycles are presented in Figure 6(B). In the beginning of oxidation process, the mass of film increases with the potential indicates that anions in the solution insert into PEDOT chain, and then the weight increase velocity of film becomes constant. On the contrary, the mass of PEDOT film decreases in reduction process due to the release of anion. The element content of Cl in the PEDOT film during reduction process is much lower than the oxidation process, while others element content have remained about the same. The main exchange anion during oxidation and reduction process is $ClO_4^-$. The energy dispersive spectroscopy (EDS) of PEDOT film undergoing oxidation and reduction process in $HClO_4$/$NaClO_4$ electrolyte are shown in Supporting Information Figure S7. Here, the mass change during the oxidation is equal to the weight loss of film during the reduction, so the reaction is totally reversible. It is obvious that the ion exchange capacity and electroactivity of UPEP S−PEDOT film is higher than that of PS PEDOT film, which is benefit from highly oriented arrangement of UPEP S−PEDOT with a sponge dendritic structure.

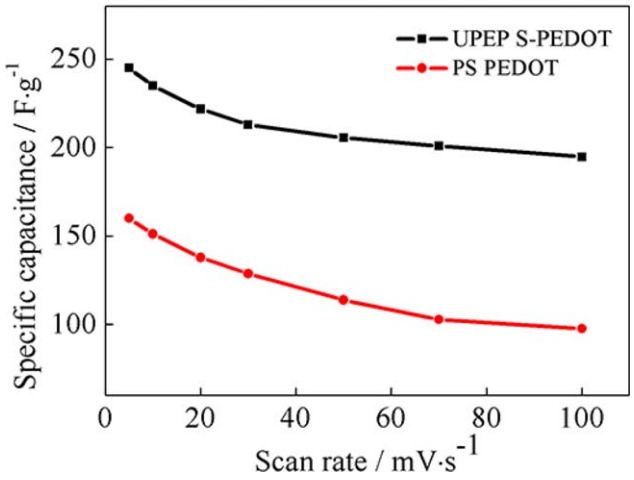


**Figure 7.** Variation in specific capacitances as a function of scan rates for UPEP S–PEDOT and PS PEDOT films. [Color figure can be viewed in the online issue, which is available at wileyonlinelibrary.com.]

Figure 7 shows the specific capacitance variation in PEDOT with scan rates varying from 10 to 100 mV $s^{-1}$. It is obvious that the specific capacitance value decreases with the gradually stabilizing trend when the scan rate is increased. At a high scan rate, diffusion of anion could be restrained, resulting in an obvious decrease in the capacitance value because the specific capacitance value strongly depends on the mobility of doping ion. In addition, the specific capacitance of UPEP S−PEDOT drops less than that of PS PEDOT during the increase in scan rate. Because UPEP S−PEDOT film was fabricated with intermittent polymerization kinetics, leading to a highly oriented b-axis arrangement separated with the doping ion, which possesses vast aligned passage for anion in molecule scale. Furthermore, the three dimensional porous structure of UPEP S–PEDOT expands the diffusion path of anion in micro scale. In this case, the spongy dendritic structure of PEDOT could

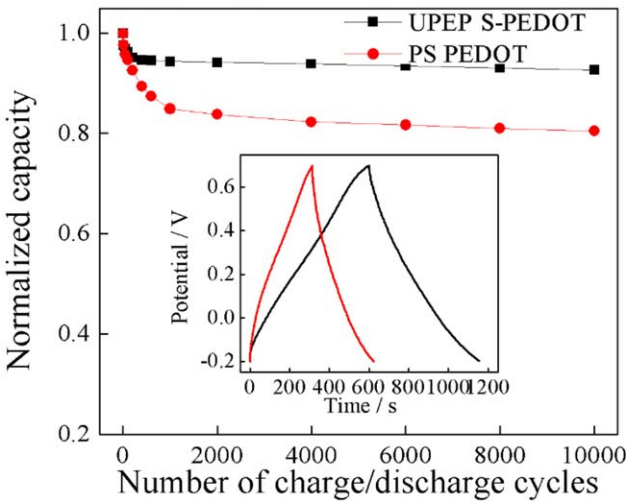


**Figure 8.** Galvanostatic charge/discharge curves of UPEP PEDOT and PS PEDOT films prepared on CNT-modified platinum substrate in three-electrode system. condition: electrolyte, 0.3 M $HClO_4$, 0.1 M $NaClO_4$; scan range, −0.2 to 0.7 V. Cycling life of UPEP S–PEDOT and PS PEDOT films under a current density of 0.7 mA $cm^{-2}$ in 0.3 M $HClO_4$, 0.1 M $NaClO_4$ aqueous solution. [Color figure can be viewed in the online issue, which is available at wileyonlinelibrary.com.]

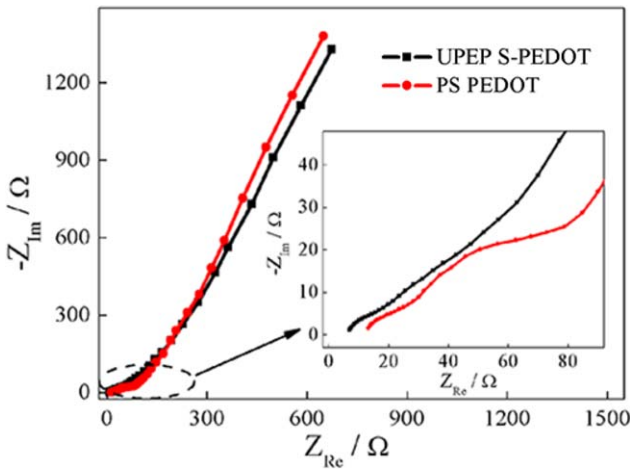


**Figure 9.** Nyquist plots of the UPEP S–PEDOT and PS PEDOT films electrodes. The inset is an enlargement of the high frequencies. [Color figure can be viewed in the online issue, which is available at wileyonlinelibrary.com.]

possess excellent electroactivity and high-speed charge–discharge properties.

**Galvanostatic Charge–Discharge Characteristics and Cycling Stability.** To further evaluate the practical performance of PEDOT film as electrode material in supercapacitor, galvanostatic charge/discharge measurements were carried out.[52] Figure 8 shows the typical galvanostatic charge/discharge curves of UPEP S−PEDOT and PS PEDOT films with an applied constant current density of 0.7 mA $cm^{-2}$ in 0.3 M $HClO_4$ and 0.1 M $NaClO_4$ aqueous solution. As seen in the inset of Figure 8, the charge/discharge curves of the PEDOT (prepared by both methods) electrodes are linear in the whole range of potential with constant slopes. A small ohm-drop phenomenon can be observed in PS PEDOT film, signifying the existence of charge transfer resistance. However, there is no ohm-drop for UPEP S−PEDOT, suggesting that it is a good material for supercapacitor. In three-electrode system, the specific capacitance is evaluated from the linear part of discharge curves, according to the following equation[53]:

$$C_m = I\Delta t / m\Delta V$$

where $C_m$, $I$, and $m$ are mass specific capacitance of active material, the applied current, and the mass of active material on the electrode, respectively. And $\Delta t$ is the time interval for the change in voltage $\Delta V$. Based on the equation, the specific capacitance of 239.1 $F{\cdot}g^{-1}$ can be obtained for the PEDOT film prepared on CNT-modified platinum by UPEP method. In contrast, the value of the specific capacitance of PS PEDOT is only 141.4 $F{\cdot}g^{-1}$. For both films, it should be noted that the total specific capacitance consists of CNTs part and main PEDOT part, in which 21.4 F $g^{-1}$ specific capacitance is contributed by CNTs as shown in Supporting Information Figure S8. The specific capacitance of S−PEDOT is much higher than PS PEDOT, which should be also due to that UPEP S−PEDOT possesses a sponge dendritic structure with larger ion exchange capacity.

The stability and reversibility of an electrode material are very important for electrochemical supercapacitor application. To evaluate the cycling stability of as-prepared UPEP S−PEDOT and PS PEDOT films, continuous galvanostatic charge–discharge measurement at a current density of 0.7 mA $cm^{-2}$ in 0.3 M $HClO_4$ and 0.1 M $NaClO_4$ aqueous solution was implemented. As shown in Figure 8, the attenuation of specific capacitance is only observed in the initial stage of galvanostatic charge–discharge measurement, then the value become almost stable. The specific capacitance of UPEP S−PEDOT exhibits an excellent cycling stability, with only 7.3% decay from its initial capacitance over 10,000 cycles. In contrast, for PS PEDOT, approximately 15.1% decay in its initial capacitance is observed in its first 1000 cycles, and about 19.5% decrease over 10,000 cycles. As stated above, the electrode capacitance could depend primarily on the growth patterns and morphology of the conducting polymer on the electrode. Here, the UPEP S−PEDOT film exhibits an excellent highly oriented arrangement in the sponge dendritic structure and shows higher electroactivity than PS PEDOT. As such, it could partly relieve volumetric stress during the galvanostatic charge–discharge cycles[54], i.e., the oxidation/reduction process, and improve the reversibility and stability of PEDOT film.

**EIS Analysis.** EIS was used to investigate the resistance limitations within the supercapacitors.[55,56] Figure 9 presents the Nyquist plots of the EIS data for the UPEP S−PEDOT and PS PEDOT films under open circuit potential (OCP) in 0.3 M $HClO_4$, 0.1 M $NaClO_4$ aqueous solution. The plot of UPEP S−PEDOT presents a typical curve of classical supercapasitor with a small distorted semicircle in high frequency region and a slanting radial in the low frequency region. At high frequencies, the diameter of semicircle pattern describes the interfacial charge transfer resistance ($R_{ct}$), which is associated with the porous structure of the electrode.[27] At low frequencies, the intercept of the semicircle on the real axis yields the solution resistance ($R_S$). In the PS PEDOT electrode, one can observe a slight increase of $R_S$, represented by the increase in the intercept of the semicircle on the real axis. Moreover, two semicircles consists of PS PEDOT $R_{ct}$ observed in high frequency region, which are associated with different ohmic phenomena occurring in the system.[54] The enlarged view of PS PEDOT is shown in the inset of Figure 9, where the first semicircle is the charge transfer from the compact internal PEDOT to the current collector; the second one is associated with the charge transfer between outer PEDOT and electrolyte interface (i.e., the actual ion doping/undoping process).[54] As stated above, the PS PEDOT film exhibits a spherical structure, in which the inner PEDOT is completely covered by the outer layer. In contrast, using UPEP method, $R_{ct}$ of S–PEDOT is much lower because

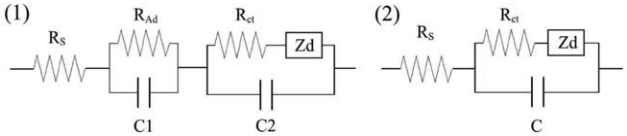


**Figure 10.** Equivalent electrical circuits for the PS PEDOT electrodes (1) and UPEP S–PEDOT electrodes (2).

the highly oriented S–PEDOT promotes the ions to move in and out freely with high electroactivity. An equivalent circuit of the proposed impedance system is presented in Figure 10. The internal PS PEDOT layer acts as an additional resistance in the form of $R_{Ad}$. The $R_{ct}$ values of UPEP S−PEDOT and PS PEDOT films are 6.74 Ω and 12.89 Ω, respectively, indicating the very low interfacial resistance in the UPEP S−PEDOT system. Details of the fitting process are presented in Supporting Information Figure S9 and Table S3. These results prove that the decrease in the impedance of UPEP S−PEDOT film is benefit from its higher ion mobility in regular crystalline laminae than that of PS PEDOT, in which the interlaminae of PS PEDOT is intercepted with each other impeding the doping process of $SDS^-$ ion.

## CONCLUSIONS

A highly oriented PEDOT film with a sponge dendritic structure has been fabricated by UPEP approach. In virtue of the cooperation of on-time and off-time pulse, the UPEP technique can produce PEDOT film with highly oriented arrangement while PS PEDOT shows random crystal alignment. Moreover, UPEP technique with intermittent polymerization kinetic results in the spongy dendritic morphology of the PEDOT films compared with a quite closely arranged globular morphology of the PS PEDOT films. Such a spongy dendritic nanostructure with highly oriented molecular arrangement improves the mass transfer rate of doping anion and relieves volumetric stress during the galvanostatic charge–discharge cycles. Therefore, the prepared PEDOT film by UPEP method can be successfully applied to electrochemical supercapacitor with outstanding electroactivity, high specific capacitances (239.1 F $g^{-1}$), and excellent cycling stability with 7.3% decay from its initial capacitance over 10,000 cycles. This material could potentially be valuable in many application fields.

## ACKNOWLEDGMENTS

This work was financially supported by the National Natural Science Foundation of China (nos. 21276173, 21306123, and 21476156), Program for the Top Young Academic Leaders of Higher Learning Institutions of Shanxi, the Foundation of the Taiyuan University of Technology for Outstanding Young Teachers (2014YQ019), and Natural Science Foundation of Shanxi Province (no. 2013021012-1).

## REFERENCES

1. Shirakawa, H.; Louis, E. J.; MacDiarmid, A. G.; Chiang, C. K.; Heeger, A. J. *J. C. S. Chem. Comm.* **1977**, 578.
2. Shi, D.; Pootrakulchote, N.; Li, R.; Guo, J.; Wang, Y.; Zakeeruddin, S. M.; Grätzel, M.; Wang, P. *J. Phys. Chem. C* **2008**, *112*, 17046.
3. Gao, M.; Xu, Y.; Bai, Y.; Jin, S. *Appl. Surf. Sci.* **2014**, *289*, 145.
4. Zhu, G.; Hou, J.; Zhu, H.; Qiu, R.; Xu, J. *J. Coat. Technol. Res.* **2013**, *10*, 659.
5. Österholm, A. M.; Shen, D. E.; Dyer, A. L.; Reynolds, J. R. *ACS Appl. Mater. Inter.* **2013**, *5*, 13432.
6. Chiang, T. Y.; Huang, M. C.; Tsai, C. H. *Appl. Surf. Sci.* **2014**, *308*, 293.
7. Zhou, C.; Liu, Z.; Yan, Y.; Du, X.; Mai, Y. W.; Ringer, S. *Nanoscale Res. Lett.* **2011**, *6*, 1.
8. Du, X.; Hao, X.; Wang, Z.; Ma, X.; Guan, G.; Abuliti, A.; Ma, G.; Liu, S. *Synth. Met.* **2013**, *175*, 138.
9. Li, Y.; Zhao, K.; Du, X.; Wang, Z.; Hao, X.; Liu, S.; Guan, G. *Synth. Met.* **2012**, *162*, 107.
10. Lee, H.; Kim, H.; Cho, M. S.; Choi, J.; Lee, Y. *Electrochim. Acta* **2011**, *56*, 7460.
11. Zhang, K.; Xu, J.; Duan, X.; Lu, L.; Hu, D.; Zhang, L.; Nie, T.; Brown, K. B. *Electrochim. Acta* **2014**, *137*, 518.
12. Wagner, M.; Lisak, G.; Ivaska, A.; Bobacka, J. *Sens. Actuators B* **2013**, *181*, 694.
13. Michalska, A.; Gałuszkiewicz, A.; Ogonowska, M.; Ocypa, M.; Maksymiuk, K. *J. Solid State Electrochem.* **2004**, *8*, 381.
14. Liu, K.; Pang, H.; Zhang, J.; Huang, H.; Liu, Q.; Chu, Y. *RSC Adv.* **2014**, *4*, 8415.
15. Zeng, H.; Jiang, Y.; Yu, J.; Xie, G. *Appl. Surf. Sci.* **2008**, *254*, 6337.
16. Groenendaal, L.; Jonas, F.; Freitag, D.; Pielartzik, H.; Reynolds, J. R. *Adv. Mater.* **2000**, *12*, 481.
17. Dietrich, M.; Heinze, J.; Heywang, G.; Jonas, F. *J. Electroanal. Chem.* **1994**, *369*, 87.
18. Jonas, F.; Krafft, W.; Muys, B. *Macromol. Symp.* **1995**, *100*, 169.
19. Jonas, F.; Heywang, G. *Electrochim. Acta* **1994**, *39*, 1345.
20. Czardybon, A.; Lapkowski, M. *Synth. Met.* **2001**, *119*, 161.
21. Kötz, R.; Carlen, M. *Electrochim. Acta* **2000**, *45*, 2483.
22. Frackowiak, E.; Beguin, F. *Carbon* **2002**, *40*, 1775.
23. Huang, J. H.; Chu, C. W. *Electrochim. Acta* **2011**, *56*, 7228.
24. Pandey, G.; Rastogi, A. *J. Electrochem. Soc.* **2012**, *159*, A1664.
25. Pandey, G.; Rastogi, A.; Westgate, C. R. *J. Power Sources* **2014**, *245*, 857.
26. Xiao, Y. M.; Lin, J. Y.; Wu, J. H.; Tai, S. Y.; Yue, G. T. *Electrochim. Acta* **2012**, *83*, 221.
27. Ryu, K. S.; Lee, Y. G.; Hong, Y. S.; Park, Y. J.; Wu, X.; Kim, K. M.; Kang, M. G.; Park, N. G.; Chang, S. H. *Electrochim. Acta* **2004**, *50*, 843.
28. Ghosh, S.; Inganäs, O. *Adv. Mater.* **1999**, *11*, 1214.
29. Patra, S.; Munichandraiah, N. *J. Appl. Polym. Sci.* **2007**, *106*, 1160.
30. Frackowiak, E.; Khomenko, V.; Jurewicz, K.; Lota, K.; Beguin, F. *J. Power Sources* **2006**, *153*, 413.
31. Ispas, A.; Peipmann, R.; Bund, A.; Efimov, I. *Electrochim. Acta* **2009**, *54*, 4668.
32. Aradilla, D.; Estrany, F.; Armelin, E.; Alemán, C. *Thin Solid Films* **2012**, *520*, 4402.
33. Patra, S.; Barai, K.; Munichandraiah, N. *Synth. Met.* **2008**, *158*, 430.

34. Skotheim, T. A. Handbook of Conducting Polymers; CRC Press, Boca Raton, Florida. **1997**.
35. Wang, Z.; Sun, S.; Hao, X.; Ma, X.; Guan, G.; Zhang, Z.; Liu, S. *Sens. Actuators B* **2012**, *171*, 1073.
36. Gupta, B.; Mehta, M.; Melvin, A.; Kamalakannan, R.; Dash, S.; Kamruddin, M.; Tyagi, A. K. *Mater. Chem. Phys.* **2014**, *147*, 867.
37. Pandolfo, A.; Hollenkamp, A. *J. Power Sources* **2006**, *157*, 11.
38. Bélanger, D.; Ren, X.; Davey, J.; Uribe, F.; Gottesfeld, S. *J. Electrochem. Soc.* **2000**, *147*, 2923.
39. Sauerbrey, G. *Zeitschrift Für Physik* **1959**, *155*, 206.
40. Sakmeche, N.; Aeiyach, S.; Aaron, J. J.; Jouini, M.; Lacroix, J. C.; Lacaze, P. C. *Langmuir* **1999**, *15*, 2566.
41. Du, X.; Wang, Z. *Electrochim. Acta* **2003**, *48*, 1713.
42. Jiang, C.; Chen, G.; Wang, X. *Synth. Met.* **2012**, *162*, 1968.
43. Atanasov, S. E.; Losego, M. D.; Gong, B.; Sachet, E.; Maria, J. P.; Williams, P. S.; Parsons, G. N. *Chem. Mater.* **2014**, *26*, 3471.
44. Han, Y.; Shen, M.; Wu, Y.; Zhu, J.; Ding, B.; Tong, H.; Zhang, X. *Synth. Met.* **2013**, *172*, 21.
45. Zhou, H.; Yao, W.; Li, G.; Wang, J.; Lu, Y. *Carbon* **2013**, *59*, 495.
46. Zhang, X.; Zhang, J.; Liu, Z. *Carbon* **2005**, *43*, 2186.
47. Kudoh, Y. *Synth. Met.* **1996**, *79*, 17.
48. Welsh, D. M.; Kloeppner, L. J.; Madrigal, L.; Pinto, M. R.; Thompson, B. C.; Schanze, K. S.; Abboud, K. A.; Powell, D.; Reynolds, J. R. *Macromolecules* **2002**, *35*, 6517.
49. Aasmundtveit, K.; Samuelsen, E.; Inganäs, O.; Pettersson, L.; Johansson, T.; Ferrer, S. *Synth. Met.* **2000**, *113*, 93.
50. Kim, T. Y.; Kim, J. E.; Suh, K. S. *Polym. Int.* **2006**, *55*, 80.
51. Zhang, L.; Wan, M.; Wei, Y. *Macromol. Rapid Commun.* **2006**, *27*, 366.
52. Sluyters-Rehbach, M.; Wijenberg, J.; Bosco, E.; Sluyters, J. *J. Electroanal. Chem.* **1987**, *236*, 1.
53. Wang, J.; Xu, Y.; Chen, X.; Du, X. *J. Power Sources* **2007**, *163*, 1120.
54. Laforgue, A. *J. Power Sources* **2011**, *196*, 559.
55. Macdonald, J. R. *J. Electroanal. Chem* **1987**, *223*, 25.
56. Macdonald, J. R. *Ann. Biomed. Eng.* **1992**, *20*, 289.